

## SIMULATIONS OF COMBUSTION ROAR IN TURBULENT ATTACHED AND LIFTED TURBULENT METHANE JET FLAMES

P. Marazioti<sup>1,2)</sup>, P. Koutmos<sup>2)</sup>

<sup>1)</sup> **Technological Education Institute (TEI)**  
**Department of Energy Technology**

Athens, Greece

<sup>2)</sup> **University of Patras**  
**Department of Mechanical and Aeronautics Engineering**

Greece 26 500

The present work presents sample results of preliminary computations of the turbulent aerothermodynamic flow field and of the noise generated by the flame front, due to turbulent fluctuations in the flame (combustion roar), in lifted and attached jet diffusion flames of methane. The two-dimensional (2D) time-dependent numerical model was built based on Reynolds-averaged Navier–Stokes (N-S) equations, equipped with the standard  $k$ - $\epsilon$  turbulence models to calculate the reacting jet flows. A reactedness – mixture fraction two-scalar exponential PDF model, based on non-premixed flame arguments, was combined with a local Damkohler number extinction criterion to delineate between the reacting and non-reacting regions. Although the inclusion of the effects of premixed flame propagation could help to improve the model, initial comparisons with experimental results suggest adequate qualitative agreement between the computations and reported data. The reasonable agreement obtained for the aerothermodynamic flame characteristics permitted a meaningful computation of the combustion noise (roar) characteristics of the studied flames, in order to address the coupled effects of heat release by the flame and turbulent interactions on the autonomous flame noise generation.

**Key words:** combustion roar, lifted flame, sound spectrum, turbulent combustion modeling.

### NOTATIONS

$\nu_t$	turbulent eddy viscosity,
$L_t$	turbulent length scale,
$k$	turbulent kinetic energy,
$\epsilon$	eddy dissipation rate,
$f$	mixture fraction,
$u$	instantaneous velocity,
$\langle u \rangle$	phase-averaged (or resolved) velocity,
$\bar{u}$	time-mean component,
$u''$	large-scale (resolved) fluctuating component,

$u'$	stochastic (subgrid) turbulent fluctuation,
$\langle u'_i u'_j \rangle$	Reynolds stresses,
$\Delta$	mesh size,
$J$	Jacobian of the transformation,
$Y$	mass fraction,
$\tau_k$	Kolmogorov time scale,
$Da_l$	local Damkohler number,
$\tau_\lambda$	turbulent time scale,
$\tau_{ch}$	chemical time scale,
$\tau_{id}$	mixing-dependent chemical ignition delay time,
$\overline{u'_j f'}, \overline{u'_j Y'_{CO_2}}$	turbulent fluxes,
$C_0$	speed of sound,
$S$	area of combustor nozzle,
$D$	laminar diffusion coefficient,
$x$	scalar dissipation,
$E_{1D}$	one-dimensional turbulence spectrum of the assumed shape,
$\theta_{f\nu}$	thickness of the mixing layer between fuel and air = $1/\sqrt{(\nabla^2 f_\nu)}$ ,
$A$	$A = [T_{\text{flame}} - T_0]/[T_{\text{flame}} f_{st} (1 - f_{st})]$ ,
$f_\nu$	frequency,
$SPL$	sound pressure level.

## 1. INTRODUCTION

Renewed interest has emerged in recent years in the study of interaction between the combustion process and the acoustics of the reacting environment [1]. Combustion roar is related to the noise generated directly by the flame due to turbulent fluctuations, independently or in combination with acoustic resonance of the reacting environment and usually involves a broadly distributed spectrum [2, 3]. The topic is of interest for practical combustor designs since it is interrelated with combustor acoustic/pressure oscillations or resonance, acoustic pollution of the environment diagnosis of operational variations and faults, and ultimately active or hybrid combustor operation control techniques [4, 5]. Practical examples which are interesting from the point of view of research on combustion roar are the combustion chambers of aircraft jet engines, flares and hot-air balloons, where minimization of flame noise is desirable.

In the present work, modeling of the autonomous noise generation by the turbulence/chemistry fluctuations in the flame front vicinity of jet diffusion flames is investigated. To describe the acoustic performance of the jet flame as an autonomous source of sound, an integral expression is employed that provides the (acoustically one-dimensional) noise spectrum of the flame, in terms of an assumed shape turbulence spectrum at the flame front, closely following the formulation put forward and derived in closed form by KLEIN [5].

As a first step towards understanding of the phenomenon, the turbulent non-premixed jet flames attached and lifted from the burner rim are studied as model problems. A diffusion flame attached to the burner nozzle lifts above the jet exit rim or blows out abruptly, when the fuel jet velocity steadily increases and exceeds the critical value. Apart from their relevance in the design and safe operation of industrial systems, such jet flame stability phenomena provide a useful research tool for experimental and numerical studies of turbulent reacting flow characteristics and related phenomena such as those presently addressed. A recent review by PITTS [6] and non-intrusive measurements by SCHEFER *et al.* [7] suggest that individual theories such as turbulent premixed flame propagation, laminar flameless quenching, large or small scale mixing, are all plausible theoretical viewpoints to describe the coupled aero-thermochemical phenomena of lift-off and blow-out.

In the described work, a 2D time-dependent phase-averaged Navier–Stokes flow simulation method [8] capable of calculating the mean and turbulent properties of the momentum and thermo-chemical fields, is employed to study the behavior of axisymmetric co-flowing methane-air jet diffusion flame configurations. Both the laminar and turbulent (lifted-off) operational conditions have been investigated to test and develop the model over a range of conditions with increasing complexity. A modular post-processor is then employed for the prediction of turbulent combustion noise, exploiting the time-mean and fluctuating thermo-chemical quantities obtained from the basic reacting flow field predictions.

## 2. NUMERICAL METHOD

### 2.1. Aerodynamic model

The reacting flows were calculated with the 2D time-dependent N-S equations governing the temporal and spatial variation of the velocities and pressures, e.g.  $u = \langle u \rangle + u'$  with  $\langle u \rangle = \bar{u} + u''$  where  $u$  and  $\langle u \rangle$  are the instantaneous and phase-averaged (or resolved) velocities,  $\bar{u}$  and  $u''$  are the time-mean and large-scale (resolved) fluctuating components and  $u'$  is the stochastic (subgrid) turbulent fluctuation. The model description given below closely follows the formulations adopted in [8]. For the reacting flows, density-weighted values are used i.e.  $\langle \tilde{f} \rangle = \frac{\rho \langle f \rangle}{\bar{\rho}}$ . The equation set may be written as follows:

$$(2.1) \quad \begin{aligned} \frac{\partial \bar{p}}{\partial t} + \frac{\partial \langle \tilde{u}_i \rangle}{\partial x_i} &= 0, \\ \frac{\partial \langle \tilde{u}_i \rangle}{\partial t} + \langle \tilde{u}_i \rangle \frac{\partial \langle \tilde{u}_i \rangle}{\partial x_j} &= -\frac{1}{\rho} \frac{\partial \bar{p}}{\partial x_i} + \frac{\partial}{\partial x_j} \left[ \nu \frac{\partial \langle \tilde{u}_i \rangle}{\partial x_j} - \langle u'_i u'_j \rangle \right] + (\bar{p} - \rho_\infty) g_i, \end{aligned}$$

with the Reynolds stresses obtained from the standard eddy-viscosity formula:

$$(2.2) \quad -\langle \overline{u'_i u'_j} \rangle = \langle \nu_t \rangle \left( \frac{\partial \langle \tilde{u}_i \rangle}{\partial x_j} + \frac{\partial \langle \tilde{u}_j \rangle}{\partial x_i} \right) - \frac{2}{3} \left[ \langle \tilde{\nu}_t \rangle \frac{\partial \langle \tilde{u}_i \rangle}{\partial x_i} + \langle \tilde{k} \rangle \right] \delta_{ij}.$$

In the conventional  $k - \varepsilon$  model,  $\langle \tilde{\nu}_t \rangle$  is related to the turbulence energy  $\langle \tilde{k} \rangle$  and its dissipation rate  $\langle \varepsilon \rangle$  as  $\langle \tilde{\nu}_t \rangle = C_\mu \langle \tilde{k} \rangle^2 / \langle \varepsilon \rangle$ , where  $\langle \tilde{k} \rangle$  and  $\langle \varepsilon \rangle$  are obtained from the standard transport equations:

$$(2.3) \quad \frac{\partial}{\partial x_j} (U_j k) = \frac{\partial}{\partial x_j} \left( \frac{\nu_t}{\sigma_k} \frac{\partial k}{\partial x_j} \right) - \overline{u_i u_j} \frac{\partial U_i}{\partial x_j} - \varepsilon,$$

$$(2.4) \quad \frac{\partial}{\partial x_j} (U_j \varepsilon) = \frac{\partial}{\partial x_j} \left( \frac{\nu_t}{\sigma_\varepsilon} \frac{\partial \varepsilon}{\partial x_j} \right) - C_{\varepsilon 1} \frac{\varepsilon}{k} \overline{u_i u_j} \frac{\partial U_i}{\partial x_j} - C_{\varepsilon 2} \frac{\varepsilon^2}{k},$$

where  $C_\mu = 0.009$ ,  $C_{\varepsilon 1} = 1.44$ ,  $C_{\varepsilon 2} = 1.92$ ,  $\sigma_k = 1.0$ ,  $\sigma_\varepsilon = 1.3$ .

The standard  $k - \varepsilon$  model has been formulated and tested within the steady-state calculation procedures, against a range of plane shear flows with no distinct peaks in their energy spectrum. When a 2D time-dependent calculation is used, part of the energy spectrum is directly resolved by this type of calculation. There is clearly a certain ambiguity as to whether the standard model is capable of partitioning the total stress into its stochastic and periodic contributions [8].

In the present time-dependent calculations, the spatial filtering due to the employed mesh is also accounted for in an effort to distinguish the directly computed (albeit 2D) turbulent motions, which are resolved by the mesh of size  $\Delta = (\Delta x \Delta y)^{1/2}$ , from the turbulence already modeled by the  $k - \varepsilon$  model.  $\langle \tilde{\nu}_t \rangle$  is therefore evaluated here by borrowing the Smagorinsky mixing length model from the large-eddy simulation (LES) formalism and the hybrid turbulence model is:

$$(2.5) \quad \langle \tilde{\nu}_t \rangle = (C_s \Delta)^2 \left( 2 \langle \tilde{S}_{ij} \rangle \langle \tilde{S}_{ij} \rangle \right)^{1/2} \quad \text{if} \quad L_t = \frac{\langle \tilde{k} \rangle^{3/2}}{\langle \tilde{\varepsilon} \rangle} > \Delta \quad \text{and}$$

$$\langle \tilde{\nu}_t \rangle = C_\mu \langle \tilde{k} \rangle^2 / \langle \tilde{\varepsilon} \rangle \quad \text{if} \quad L_t < \Delta.$$

$C_s$  is taken as 0.1. The resulting  $\tilde{\nu}_t$  is fed back into the production of  $\langle \tilde{k} \rangle$  in the  $k - \varepsilon$  equations, thereby producing a continuous distribution of  $\nu_t$ . The implicit scheme used here is therefore well suited for this hybrid formulation. Calculations with the standard  $k - \varepsilon$  model have been proven clearly to be inferior to the recent hybrid method predictions, both for cold and reacting bluff-body flows, what has been demonstrated in KOUTMOS *et al.* [8].

## 2.2. Combustion model

2.2.1. *Basic turbulence/chemistry interaction model.* A partial equilibrium scheme corresponding to a two-scalar description employing the mixture fraction,  $f$ , and the  $\text{CO}_2$  concentration,  $Y_{\text{CO}_2}$ , were used. The reaction  $\text{CO} + \text{OH} \leftrightarrow \text{CO}_2 + \text{H}$  was introduced to allow for non-equilibrium effects, and  $\text{CO}_2$  formation from  $\text{CO}$  is assumed to proceed as:

$$\dot{r}_{\text{CO}_2} = k_f Y_{\text{CO}} Y_{\text{OH}} - \left( \frac{k_f}{k_\varepsilon} \right) Y_{\text{CO}_2} Y_{\text{H}}, \quad k_f = 6.76 \cdot 10^{11} \exp \left( \frac{T}{1102} \right)$$

and  $k_\varepsilon$  is taken from the JANAF (Tables).

Additionally, when the mixture strength exceeds the rich flammability limit, the composition is taken as that of equilibrium at this limit diluted with pure fuel. The final composition is calculated from the NASA equilibrium code for given  $f$  and  $Y_{\text{CO}_2}$  values by defining  $Y_{\text{CO}_2}$  as an ‘element’. The passive,  $f$ , and the reactive,  $Y_{\text{CO}_2}$ , variables, are calculated from the equations

$$(2.6) \quad \frac{\partial (\bar{\rho} \langle \tilde{f} \rangle)}{\partial t} + \frac{\partial}{\partial \chi_j} (\bar{\rho} \langle \tilde{u}_j \rangle \langle \tilde{f} \rangle) = \frac{\partial}{\partial \chi_j} \left[ \left( \bar{\rho} D + \frac{\mu_t}{Sc_t} \right) \frac{\partial \langle \tilde{f} \rangle}{\partial \chi_j} \right],$$

$$(2.7) \quad \frac{\partial (\bar{\rho} \langle \tilde{Y}_{\text{CO}_2} \rangle)}{\partial t} + \frac{\partial}{\partial \chi_j} (\bar{\rho} \langle \tilde{u}_j \rangle \langle \tilde{Y}_{\text{CO}_2} \rangle) = \frac{\partial}{\partial \chi_j} \left[ \left( \bar{\rho} D + \frac{\mu_t}{Sc_t} \right) \frac{\partial \langle \tilde{Y}_{\text{CO}_2} \rangle}{\partial \chi_j} \right] + \bar{\rho} \tilde{r}_{\text{CO}_2},$$

with gradient transport assumptions for the turbulent fluxes  $\overline{u'_j f'}$  and  $\overline{u'_j Y'_{\text{CO}_2}}$ .

An exponential joint PDF is constructed from the normalized mixture fraction and  $\text{CO}_2$  concentration values,  $f^*$  and  $Y_{\text{CO}_2}^*$ , which are used to transform the physically allowable space of  $f$  and  $Y_{\text{CO}_2}$  into a normalized square area suitable for integration. The relationships established by this transformation are:

$$(2.8) \quad f^* = f + Y_{\text{CO}_2} / Y_{\text{CO}_2, \text{air}}, \quad Y_{\text{CO}_2}^* = Y_{\text{CO}_2} / (f Y_{\text{CO}_2, \text{fuel}}),$$

where

$$Y_{\text{CO}_2, \text{fuel}} = n M_{\text{CO}_2} / M_{\text{C}_n \text{H}_M},$$

$$Y_{\text{CO}_2, \text{air}} = M_{\text{CO}_2} / (M_{\text{O}_2} + M_{\text{N}_2} / 0.259).$$

The local PDF is of the form:

$$(2.9) \quad P(f^*, Y_{\text{CO}_2}^*) = \exp[a_1 + a_2 f^* + a_3 Y_{\text{CO}_2}^* + a_4 f^{*2} + a_5 Y_{\text{CO}_2}^* + a_6 f^* Y_{\text{CO}_2}^*],$$

where  $f^*$  and  $Y_{\text{CO}_2}^*$  are appropriately transformed variables, and it is calculated through the coefficients  $(a_1 \dots a_6)$  which depend on the local moments  $\overline{f'^2}$ ,  $\overline{Y_{\text{CO}_2}'^2}$ ,  $\overline{f'Y_{\text{CO}_2}'}$ , which are obtained by assuming equilibrium between the turbulent production and destruction of these moments in their transport equation:

$$(2.10) \quad \frac{\partial (\overline{\rho X'Z'})}{\partial t} + \frac{\partial (\overline{\rho \tilde{u}_j X'Z'})}{\partial x_j} = \frac{\partial}{\partial x_j} \left[ \left( \overline{\rho D} + \frac{\mu_t}{Sc_t} \right) \frac{\partial \overline{X'Z'}}{\partial x_j} \right] \\ + 2 \frac{\mu_t}{Sc_t} \left[ \frac{\partial \tilde{X}}{\partial x_i} \frac{\partial \tilde{Z}}{\partial x_i} \right] - C_\Phi \overline{\rho} \frac{1}{\tau_t} \overline{X'Z'} + \overline{X'S_Z} + \overline{Z'S_X}.$$

The moments are then obtained from the following expression:

$$(2.11) \quad \overline{X'Z'} = \frac{1}{2.0\overline{\rho}} \left[ \frac{2\mu_t}{Sc_t} \frac{\partial \tilde{X}}{\partial x_i} \frac{\partial \tilde{Z}}{\partial x_i} + \overline{X'S_Z} + \overline{Z'S_X} \right] \tau_t,$$

$$\overline{X} = \langle \tilde{f} \rangle \quad \text{or} \quad \langle \tilde{Y}_{\text{CO}_2} \rangle \quad \text{and} \quad \overline{Z} = \langle \tilde{f} \rangle \quad \text{or} \quad \langle \tilde{Y}_{\text{CO}_2} \rangle, \quad C_\Phi = 2.0.$$

Mean quantities and correlations are evaluated by using the PDF information, e.g.

$$(2.12) \quad \tilde{r}_{\text{CO}_2} = \frac{1}{\overline{\rho}} \iiint \tilde{r}_{\text{CO}_2} J \rho P(f^* \tilde{Y}_{\text{CO}_2}^*) df^* dY_{\text{CO}_2}^*,$$

where  $J$  is the Jacobian of the transformation,  $\tau_t$  is evaluated as follows in line with the hybrid model formulation: if  $L_t > \Delta$  then  $\tau_t = \Delta / \sqrt{\langle \tilde{k} \rangle}$ , and if  $L_t < \Delta$  then  $\tau_t = \langle \tilde{k} \rangle / \langle \tilde{\varepsilon} \rangle$ .

*2.2.2. Extinction/reignition model.* The modeling of finite-rate chemistry effects such as partial extinctions and reignitions encountered in the lifted flames follows the approach of KOUTMOS [9]. Local extinction is predicted when the local Damkohler number,  $Da_l$ , defined as the ratio of the turbulent time scale  $\tau_\lambda = 3.88\tau_k$  ( $\tau_k$  is the Kolmogorov time scale) to the chemical time scale,  $\tau_{ch}$ , is below the local critical ‘limit’  $Da_{cr}$  being a function of position and local conditions. The criterion for local quenching reads then:

$$(2.13) \quad \lambda = \frac{Da_l}{Da_{cr}} = \frac{[\tau_\lambda / \tau_{ch}]}{\left[ \frac{\Sigma_f}{\sqrt{2}\Delta f_R} R_{e_t}^{1/4} \right]} \leq 1.$$

The mean gas state subsequent to extinction  $\tilde{Y}_Q$  is obtained by convoluting with the local exponential PDF involving the reactedness,  $B$ , and the mixture fraction:

$$(2.14) \quad \tilde{Y}_Q = (1/\tilde{\rho}) \iint Y_Q \rho P(\tilde{f}, \tilde{B}) df dB,$$

$\tilde{B}$  is here calculated from the following model Lagrange-type transport equation [10]:

$$(2.15) \quad \frac{\partial (\rho \tilde{B})}{\partial t} + \frac{\partial (\tilde{\rho} \tilde{u}_j \tilde{B})}{\partial \chi_j} = S_B,$$

while its fluctuations,  $\tilde{B}^2$  and  $\tilde{f}\tilde{B}'$ , are obtained by invoking a scale-similarity assumption [12]. Further details of the full model may be found in Refs. [8, 9, 12].

Reignition is allowed when a) the time-scale criterion, Eq. (2.13), is inoperative and b) the cumulative probability of finding a flammable mixture at this location, defined as

$$P_F = \int_{f_1}^{f_2} P(f^*) df^*,$$

is greater than 0.65. Then the source term in Eq. (2.15) is equal to

$$(B_0 - \tilde{B})/\tau_{id},$$

where  $\tau_{id}$  is a mixing-dependent chemical ignition delay time [8–12].

### 2.3. Turbulent flame noise model

For evaluation of the autonomous sound radiation due to interaction of the turbulent fluctuations with the flame front, the model formulation of KLEIN [5] has been followed closely. Starting from the basic wave equation for low Mach number flows [1, 2], the one-dimensional sound generated by the fluctuating heat release from a turbulent non-premixed flame is evaluated [5] by deriving an integral expression, assuming that the instantaneous combustion zone is infinitely thin and that combustion is fast and determined by mixing of fuel and air. The sound spectrum can then be expressed [5] as a function of a one-dimensional turbulence spectrum (of assumed shape) of the mixture fraction at the flame front. The resulting expression for the sound spectrum for a non-premixed turbulent flame is then given in integral form as a function of frequency:

$$(2.16) \quad pp(f_\nu) = 2\pi \left(\frac{C_0}{S}\right)^2 \iint_{\mathbf{x}} \left[ (\rho D B A)^2 \frac{L_{\text{cor}} \theta_{f_\nu}}{2U} E_{ID}^2 \left(\frac{2\pi f_\nu}{2U}\right) \right] dx dy,$$

where  $C_0$  – speed of sound,  $S$  – area of combustor nozzle,  $D$  – laminar diffusion coefficient  $B$ ,

$$B = \frac{1}{2}x \left/ \frac{1}{\pi} D \int_0^{\infty} E_{ID}(k) dk, \right.$$

$x$  – scalar dissipation =  $2.0 \frac{\varepsilon}{k} \tilde{f}'_{\nu}{}^2$ ,  $E_{ID}$  – one-dimensional turbulence spectrum of assumed shape,

$$E_{ID} = \left\{ \begin{array}{ll} 1, & k_1 < k_{\varepsilon} \\ (k_1/k_2)^{-(5/3)}, & k_{\varepsilon} < k_1 < k_{kol} \\ 0, & k_1 > k_{kol} \end{array} \right\}$$

with  $k_1 = 2\pi f_{\nu}/2U$ ,  $k_{\varepsilon} = \pi/l_t$ ,  $k_{kol} = (\varepsilon/\nu^3)^{1/4}$ ,  $\theta_{f_{\nu}}$  – thickness of the mixing layer between fuel and air, equal to  $1/\sqrt{(\nabla^2 f_{\nu})}$ ,

$$A = [T_{\text{flame}} - T_0]/[T_{\text{flame}} f_{st} (1 - f_{st})],$$

$f_{\nu}$  – frequency.

The parameter sound pressure level,  $SPL$ , expressed in dB, can also be evaluated as:

$$(2.17) \quad SPL(f_{\nu}) = 20 \log \left( \frac{\sqrt{pp(f_{\nu})}}{20 \cdot 10^{-6}} \right).$$

The time-averaged information about the turbulence sound spectrum and other parameters required in the above expression is derived from the basic reacting flow calculation, the computation of the sound spectrum being performed in a post-processing step.

#### 2.4. Numerical details

The coflowing methane-air jet configuration and computational domain are shown in Fig. 1. The convective condition  $\partial\phi/\partial t + U_0(\partial\phi/\partial x) = 0$ , ( $C = \bar{U}_0$ ) was used at the outlet. A mesh of  $205 \times 123$  ( $x, y$ ) grid points was used with an axial expansion ratio of 1.1. For inlet conditions, a fully developed flow was assumed.

The equations were solved using a finite-volume method based on a staggered mesh, a pressure correction method (SIMPLE) and the QUICK differencing scheme [8]. A second-order scheme was used for temporal integration. Time steps were of the order  $10^{-4} - 10^{-5}$  sec, depending on the fuel Reynolds number. After an initial transient of about  $30t_0$  ( $t_0 = D/U_0$ ), the statistics were computed over approximately  $100t_0$ .

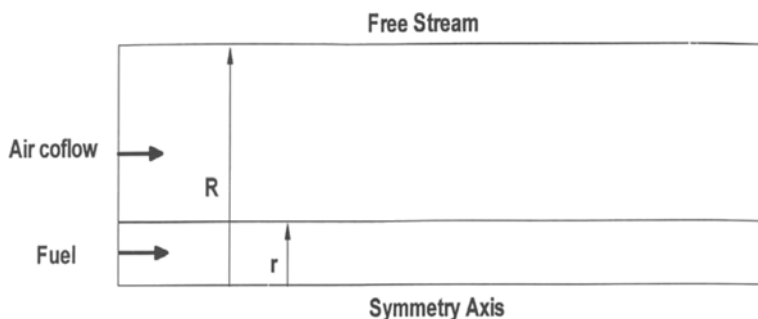


FIG. 1. Methane-air coflowing jet flame configuration Investigated  $R = 27r$  and the length of computation Domain is  $50r$ .

### 3. RESULTS AND DISCUSSION

Computations were initially performed for a steady-state, laminar  $\text{CH}_4$ -air diffusion flame for which experimental data by MITCHELL *et al.* [13] is available. Figures 1 and 2 show the flow configuration and sample results for undiluted  $\text{CH}_4$  jet flow at 5 cm/sec through a 1.2 cm-diameter tube, with a coflow of air at 10 cm/sec, which are compared against the experimental data of reference [13]. Results are compared with the data at the final steady-state, which was reached after about 25,000 time-steps ( $\Delta t = 0.06$  sec). Overall, the agreement is satisfactory in both the reactive scalar (temperature) and the momentum field (axial velocity), despite some experimental uncertainties concerning the rig exit conditions and these comparisons lend support for an extension of the basic model to more complex, turbulent lifted flames.

Figure 3 displays time-averaged temperature contours for the three jet velocities of 2, 20 and 40 m/sec investigated. The stoichiometric contour is also superimposed on the plot. By comparison to the reported non-dimensional lift-off heights, the present simulation seems to underestimate the stabilization position by about 7% and 12% for the two jet velocities respectively. An instantaneous isotherm snapshot of the reacting flow field is illustrated in Fig. 4. A variation of the lifted flame base with an up and down movement of about 12%, was observed in the time-dependent simulations. Due to their two-dimensional nature, the resulting spectra could not allow a reliable evaluation of the spectral behavior of this important lifted flame base region.

An overall qualitative picture of the velocity field is shown in the form of vector plots in Fig. 5. The mean velocity (Favre-averaged) due to expansion slows down approaching the flame front and accelerates as it flows past it. Any relevant local scaling is therefore expected to include the effects of expansion on local parameters, e.g. the flame front propagation speed in relation to the laminar flame speed.

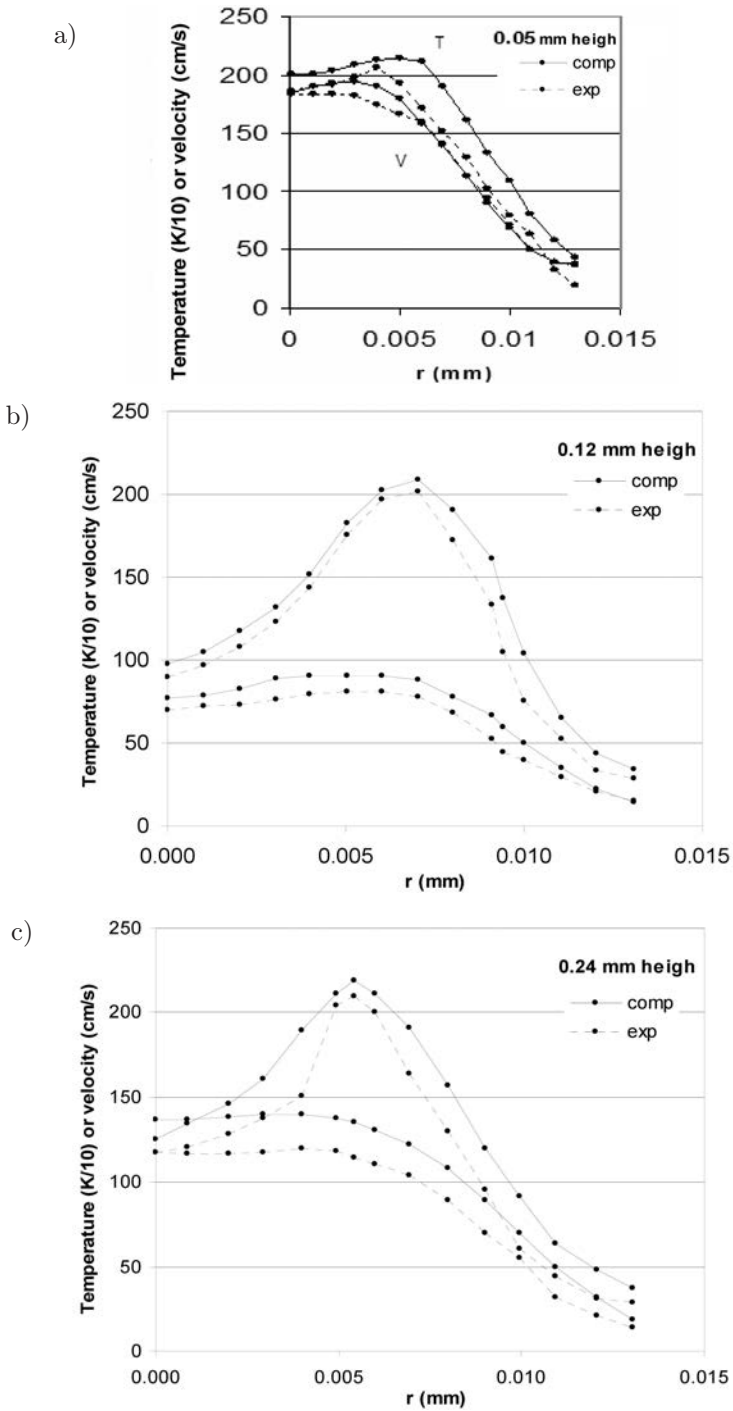


FIG. 2. Laminar CH<sub>4</sub> jet flame predictions for fuel jet velocity a) 2 m/s, b) 20 m/s, c) 40 m/s.

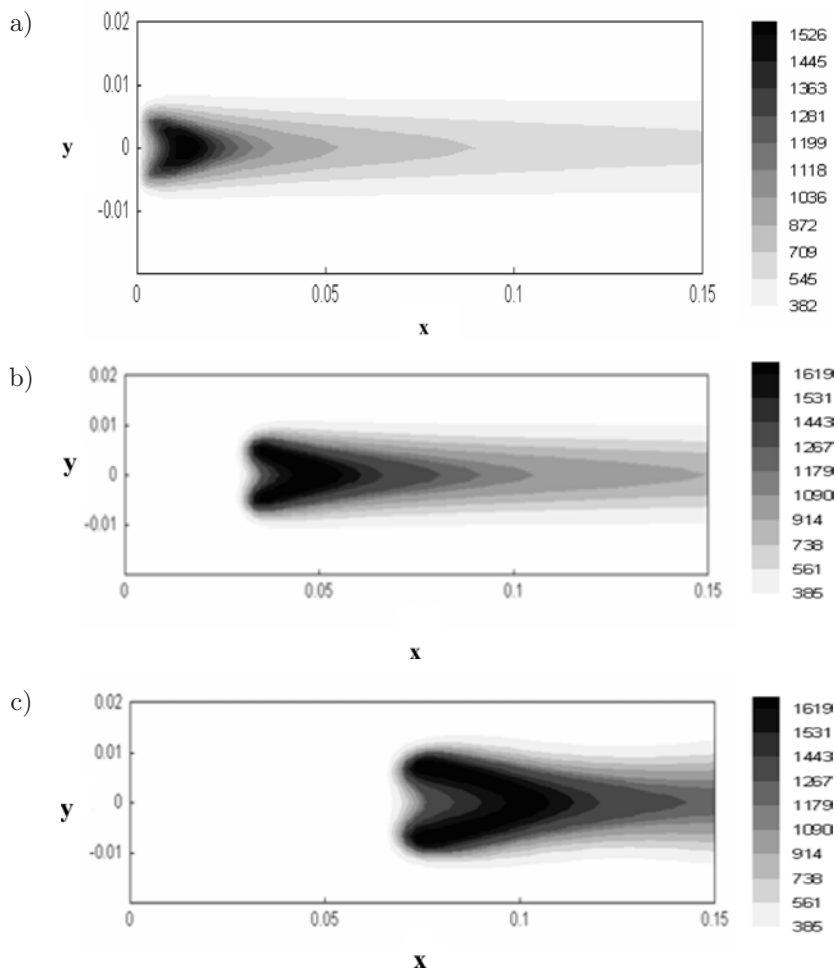
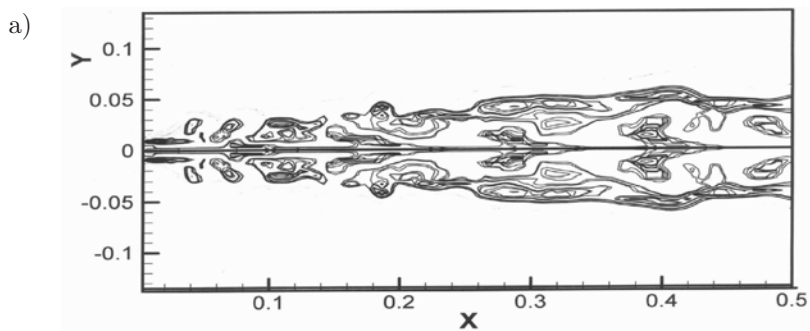


FIG. 3. Time-average temperature contours for fuel jet velocity a) 2 m/s, b) 20 m/s, c) 40 m/s.



[Fig. 4a]

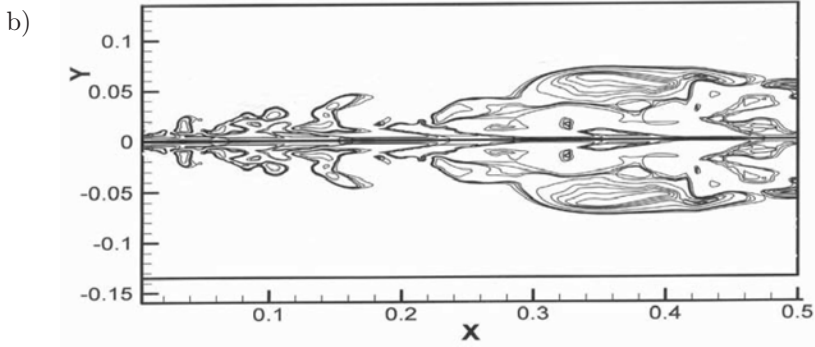
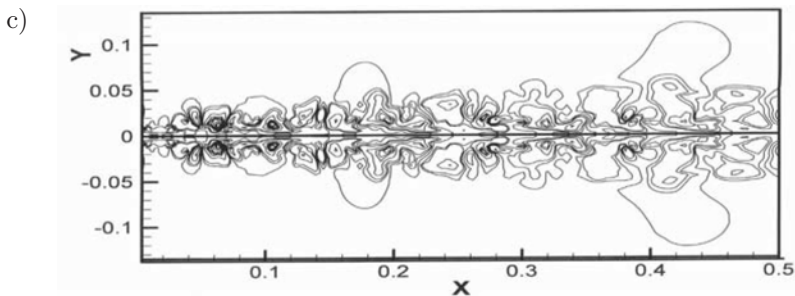
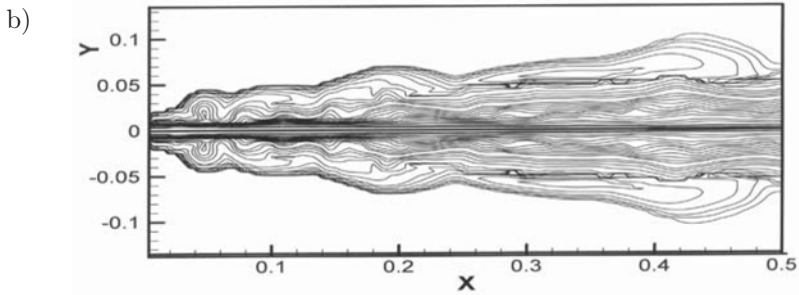
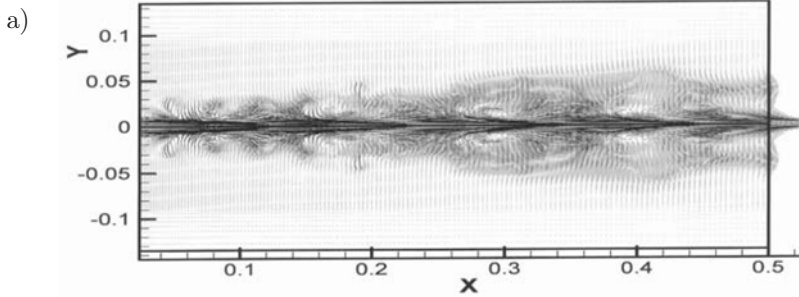


FIG. 4. Instantaneous temperature isotherms: a)  $u_j = 20$  m/s, b)  $u_j = 40$  m/s.



[Fig. 5a, b, c]

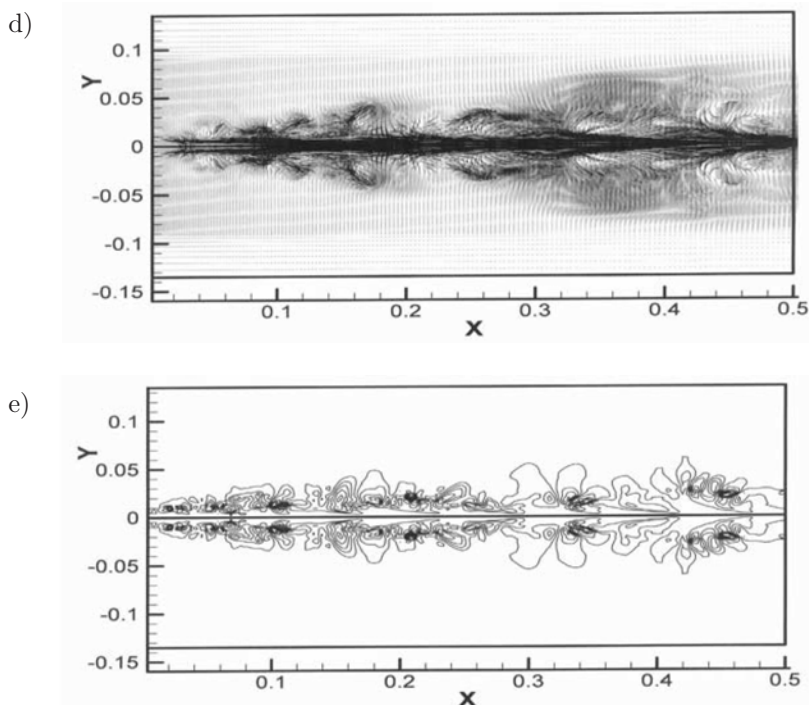


FIG. 5. a) Instantaneous plot of velocity vectors ( $u_j = 20$  m/s); b) instantaneous plot of fuel fraction contours ( $u_j = 20$  m/s); c) instantaneous plot of V contours ( $u_j = 20$  m/s); d) instantaneous plot of velocity vectors ( $u_j = 40$  m/s); e) instantaneous plot of V contours ( $u_j = 40$  m/s).

Some preliminary joint statistics between temperature and mixture fraction, two important scaling parameters for the partially premixed regime [14], have been produced from the time-dependent calculation of the higher fuel jet velocity of 20 m/sec and they are shown in Fig. 6. The collected points lie close to the stoichiometric contour in the vicinity of the movement of the flame base. Methane is well-known for its bimodal approach to extinction from a wide range of the previously reported papers (e.g. [12]). The present plot implies a lower level of bimodality, with the scatter points located mostly above the mixing asymptote and below the partial equilibrium levels. The variance of mixture fraction spreads the points over an area slightly broader than the lean limit.

Experimental data of this nature would be very helpful in identifying the detailed nature and flow behavior of the near-stabilization region. The reduced bimodality with respect to customary diffusion flames [12, 14] may be attributed to the loss of resolution in the present simulation, to deficiencies in the reignition model which is formulated for pure diffusion flames, or to a lower variability of the chemical time-scale arising from omission of the effects of partially premixed

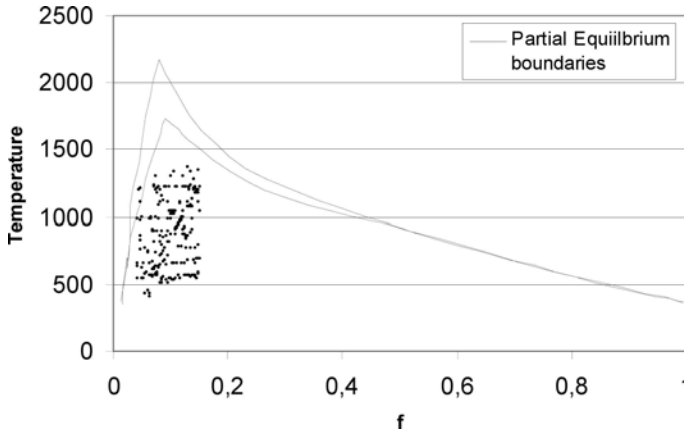


FIG. 6. Mixture fraction-Temperature scatter plot taken in the vicinity of the lifted flame base.

flame propagation. This aspect is not treated explicitly in the model other than through the inclusion of the relevant chemical time-scale.

Encouragingly, the present modeling formulation recovered two important, experimentally observed trends. Firstly, the linear relationship between the flame lift-off height and jet exit velocity, that has been extensively verified through global and detailed measurements, as well as the correct slope of this linear variation. Secondly, it reproduced adequately the increase in lift-off height for a given jet inflow velocity as the fuel flow is diluted, e.g. with  $N_2$ , something expected since the residence time is now longer when the fuel stream is diluted.

The reasonable performance of the computational model of prediction of the experimentally observed aerothermodynamic parameter variations and trends, lends support to the extension of the method to include and apply the flame noise described previously, to enable a meaningful evaluation of the combustion noise radiated by the present flames. Flame noise calculations were performed for two selected flame configurations, the attached flame with exit fuel velocity of 2 m/s and the lifted-off flame configuration with exit fuel velocity of 20 m/s.

Equation (2.16) was discretized to be able to calculate it numerically and the integral is computed numerically at every grid cell. The part in square brackets in the expression of Eq. (2.16) can be considered as the strength of the local noise source and gives an indication of a spatial distribution of the local noise ‘intensity’ in the reacting flow field for each selected frequency. Integrating numerically Eq. (2.16) for all cell surface and over the full frequency range ( $\Delta f_\nu = 1$  Hz,  $P_{\text{ref}} = 20 \mu\text{Pa}$ ), we deduce the sound spectrum expressed in dB sound pressure level from Eq. (2.17). The turbulent aero-thermochemical data produced by the basic time-dependent computation are time-averaged and supply the required information necessary to evaluate the parameters involved in Eq. (2.16) for every

cell surface and frequency. Figures 7a, b display contours of the local noise intensity (the term between the square brackets in Eq. (2.16)) for a frequency of 100 Hz.

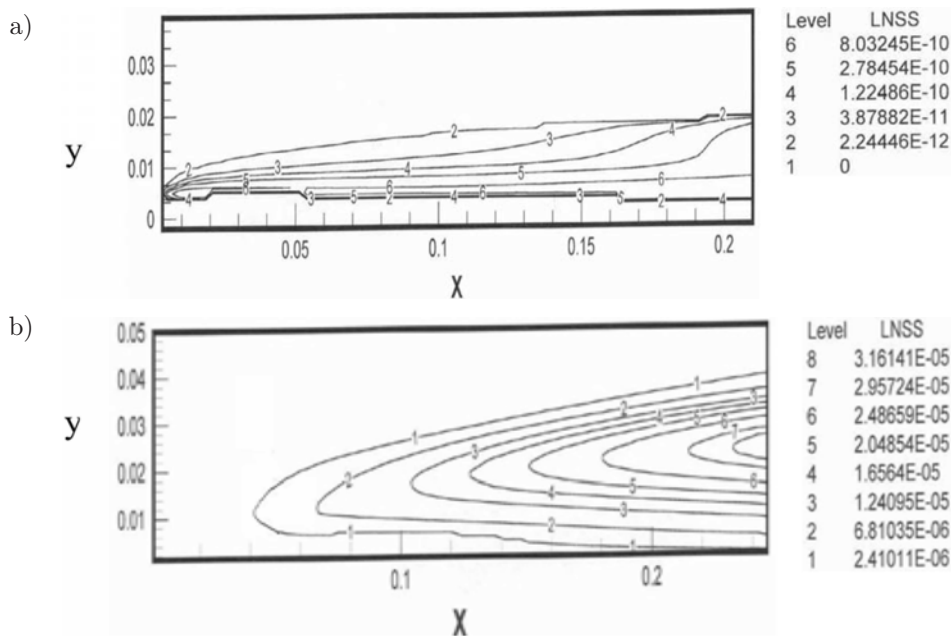


FIG. 7. The local noise source intensity distribution for fuel jet velocity: a) 2 m/s, b) 20 m/s.

It is seen that noise generation levels are predominant mainly in vicinity of the mixing interface between the fuel and the oxidizer. These attain maximum values downstream of the lift-off flame base for the lifted flame, while for the attached flame the peak noise strength region is again dislocated downstream of the burner rim. In both cases, the location of the maximum noise intensity coincides with the region of the peak temperatures levels. The lifted flame produces significantly increased maximum values of the local noise source strength with respect to the attached flame and this appears to be a reasonably predicted trend, since the lifted flame produces increased turbulence levels and temperature fluctuations downstream of its lifted base.

The calculated sound spectra for the above-discussed flames are plotted in Figs. 8a, b. The lifted flame gives elevated energy content in the sound spectrum by about 30% with respect to the attached case, particularly near the lower frequency range at about 80 Hz, thereafter falling off to nearly similar levels. This is evidently consistent with the previously discussed predictions of the local noise intensity levels. It should also be noted that the qualitative distribution of the spectral density also depends on the assumed turbulence spectrum used in Eq. (2.16).

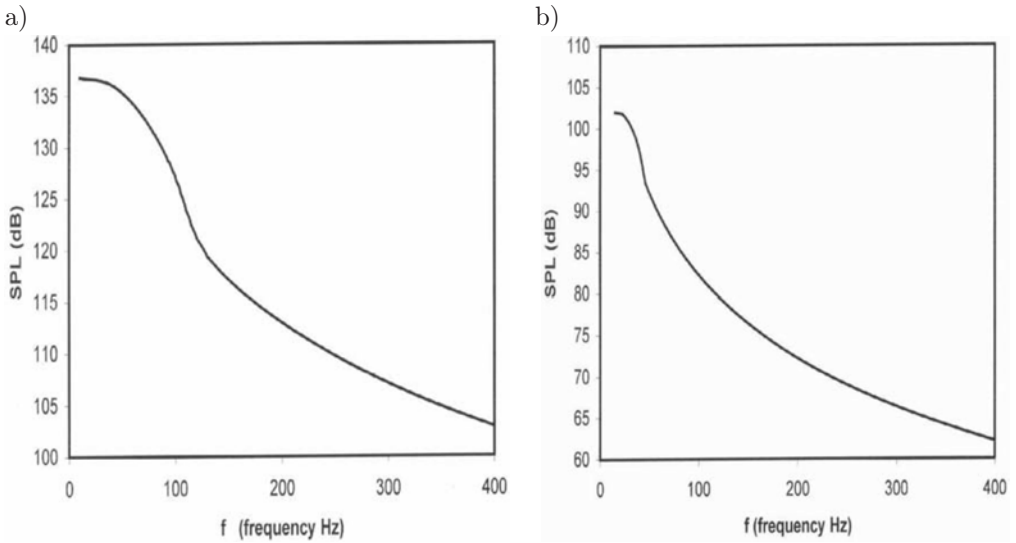


FIG. 8. The calculated sound spectra for: a) lifted and b) attached flame, plotted in SPL dB ( $\Delta f = 1$  Hz).

An aspect that merits discussion is whether the assumption of fast chemistry can still be applied for the partially-premixed flame configuration with lift-off when using Eq. (2.15), and to what extent the expected discrepancies affect the validity of the present prediction. Experimental results would be quite helpful to identify the extent of disagreement in the sound pressure level predictions of this flame and this would help to improve the present modeling effort. Notwithstanding the above arguments, it is believed that the present procedure has captured the basic behaviors and trends in the aero-thermochemical and flame noise generation characteristics of the studied flames, although further tests and refinements would be required to enlarge the applicability of the method.

#### 4. SUMMARY

A computational procedure of the time-dependent reactive Navier–Stokes equations has been employed to study the stabilization mechanism and the autonomous noise generation by the flame front, due to turbulent fluctuations in attached and lifted methane jet flames. Although the method exploited primarily the diffusion flame concepts with the effects of partial extinctions/reignitions embodied, it produced reasonable qualitative agreement with the reported data. Despite the fact that these exploratory and preliminary computations are based on axisymmetric configurations and hence the 3-D or the non-symmetric turbulent behavior is excluded, the present method captured many important trends

and behaviors and allows for evaluation and further development of the overall methodology. Further extensions along the line of addressing in a more clear-cut manner the impact of partial-premixing are also required.

The adequate accord between computations and experimental observation in the turbulent aerothermodynamic flow and flame parameters enabled a first attempt to evaluate the turbulent combustion noise (roar) characteristics of the complex flame configurations investigated here. The developed methodology provides a basis to address the coupled effects of turbulence interactions, heat release and chemistry, and the autonomous turbulent combustion noise generated at the flame front. These preliminary results suggest that the modeling procedure followed such complex behaviors as the variation of the flame lift-off height with fuel jet velocity and the accompanying increase of the radiated flame noise levels. Further detailed assessment and improvements of the described methodology may however be required to demonstrate its wider applicability.

#### ACKNOWLEDGMENT

The research was sponsored by the program “K. Karatheodori”, Epitropi Ereunon, University of Patras.

#### REFERENCES

1. J. M. TRUFFAUT, G. SEARBY and L. BOYER, *Sound emission by non-isomolar combustion at low Mach numbers*, Combustion Theory and Modeling, **2**, 423–428, 1998.
2. S. M. CANDEL, *Combustion instabilities coupled by pressure waves and their active control*, Proc. Combustion Institute, **24**, 1277–1296, 1992.
3. W. C. STRAHLE, C. CASCI and C. BRUNO, *Recent Advances in the Aerospace Sciences*, (New York: Plenum) 103–140, 1985
4. P. BOIENAU, Y. GERRAIS and V. MORICE, *An aerothermoacoustic model for computation of sound radiated by turbulent flames*, Internoise, **96**, 495–508, 1996.
5. S. A. KLEIN, *On the acoustics of turbulent non-premixed flames*, PhD thesis, University of Twente, Enschede, The Netherlands, 2000.
6. W. M. PITTS, *Assessment of the theories for the behaviour and blow-out of lifted turbulent jet diffusion flames*, 22nd Symposium (International) on Combustion, The Combustion Institute, Pittsburgh, 809–816, 1989.
7. R. W. SCHEFER, M. NAMAZIAN, E. E. J. FILTOPOULOS and J. KELLY, *Temporal evolution of turbulence/chemistry interactions in lifted turbulent-jet flames*, 25th Symposium (International) on Combustion, The Combustion Institute, Pittsburgh, 1223–1231, 1994.
8. P. KOUTMOS, C. MAVRIDIS and D. PAPAILIOU, *Time-dependent computation of turbulent bluff-body diffusion flames close to extinction*, International Journal of Numerical Methods for Heat and Fluid Flow, **9**, 39–59, 1999.

9. P. KOUTMOS, *Damkohler number description of local extinction in turbulent methane jet diffusion flames*, *Fuel*, **78**, 623–626, 1999.
10. R. BORGHİ, *Turbulent combustion modeling*, *Prog. in Energy and Combustion Science*, **14**, 245–292, 1988.
11. P. KOUTMOS and P. MARAZIOTI, *Identification of local extinction topology in axisymmetric bluff-body diffusion flames with a reactedness-mixture fraction presumed probability density function model*, *International Journal for Numerical Methods in Fluids*, **35**, 939–959, 2001.
12. D. PAPAILIOU, P. KOUTMOS, C. MAVRIDIS and A. BAKROZIS, *Simulations of local extinction phenomena in bluff-body stabilized diffusion flames with a Lagrangian reactedness model*, *Combustion Theory and Modelling*, **3**, 409–431, 1999.
13. R. E. MITCHELL, A. F. SAROFIN and L. A. CLOMBURG, *Experimental and numerical investigation of confined laminar diffusion flames*, *Combustion and Flame*, **37**, 227–244, 1980.
14. T. ECHEKKI and J. H. CHEN, *The effects of complex chemistry on triple flames*, NASA CTR manuscript, *Proceedings of the Summer School*, 217–233, 1996.

*Received May 27, 2009.*

---